

Physiological noise in murine solid tumours using T2*-weighted gradient-echo imaging: a marker of tumour acute hypoxia?

Christine Baudalet^{1,2}, Réginald Ansiaux¹, Bénédicte F Jordan^{1,2},
Xavier Havaux³, Benoit Macq⁴ and Bernard Gallez^{1,2,5}

¹ Laboratory of Biomedical Magnetic Resonance, Université Catholique de Louvain, Brussels, Belgium

² Laboratory of Medicinal Chemistry and Radiopharmacy, Université Catholique de Louvain, Brussels, Belgium

³ Cardiovascular Pathology Unit, Université Catholique de Louvain, Brussels, Belgium

⁴ Communications and Remote Sensing Unit, Université Catholique de Louvain, Louvain-La-Neuve, Belgium

E-mail: gallez@cmfa.ucl.ac.be

Received 15 October 2003, in final form 10 May 2004

Published 9 July 2004

Online at stacks.iop.org/PMB/49/3389

doi:10.1088/0031-9155/49/15/006

Abstract

T2*-weighted gradient-echo magnetic resonance imaging (T2*-weighted GRE MRI) was used to investigate spontaneous fluctuations in tumour vasculature non-invasively. FSa fibrosarcomas, implanted intramuscularly (i.m.) in the legs of mice, were imaged at 4.7 T, over a 30 min or 1 h sampling period. On a voxel-by-voxel basis, time courses of signal intensity were analysed using a power spectrum density (PSD) analysis to isolate voxels for which signal changes did not originate from Gaussian white noise or linear drift. Under baseline conditions, the tumours exhibited spontaneous signal fluctuations showing spatial and temporal heterogeneity over the tumour. Statistically significant fluctuations occurred at frequencies ranging from 1 cycle/3 min to 1 cycle/h. The fluctuations were independent of the scanner instabilities. Two categories of signal fluctuations were reported: (i) true fluctuations (TFV), i.e., sequential signal increase and decrease, and (ii) profound drop in signal intensity with no apparent signal recovery (SDV). No temporal correlation between tumour and contralateral muscle fluctuations was observed. Furthermore, treatments aimed at decreasing perfusion-limited hypoxia, such as carbogen combined with nicotinamide and flunarizine, decreased the incidence of tumour T2*-weighted GRE fluctuations. We also tracked dynamic changes in T2* using multiple GRE imaging. Fluctuations of T2* were observed; however, fluctuation maps using PSD analysis could not be generated reliably. An echo-time dependency

⁵ Address for correspondence: CMFA/REMA Units, Université catholique de Louvain, Avenue E. Mounier 73.40, B-1200 Brussels, Belgium.

of the signal fluctuations was observed, which is typical to physiological noise. Finally, at the end of T2*-weighted GRE MRI acquisition, a dynamic contrast-enhanced MRI was performed to characterize the microenvironment in which tumour signal fluctuations occurred in terms of vessel functionality, vascularity and microvascular permeability. Our data showed that TFV were predominantly located in regions with functional vessels, whereas SDV occurred in regions with no contrast enhancement as the result of vessel functional impairment. Furthermore, transient fluctuations appeared to occur preferentially in neoangiogenic hyperpermeable vessels. The present study suggests that spontaneous T2*-weighted GRE fluctuations are very likely to be related to the spontaneous fluctuations in blood flow and oxygenation associated with the pathophysiology of acute hypoxia in tumours. The disadvantage of the T2*-weighted GRE MRI technique is the complexity of signal interpretation with regard to pO₂ changes. Compared to established techniques such as intravital microscopy or histological assessments, the major advantage of the MRI technique lies in its capacity to provide simultaneously both temporal and detailed spatial information on spontaneous fluctuations throughout the tumour.

(Some figures in this article are in colour only in the electronic version)

Introduction

Over the past decade, the understanding of the origin of oxygen deficiency in solid tumours has evolved considerably. Tumour hypoxia in tumours can be classified into two types: chronic hypoxia and acute hypoxia. Chronic hypoxia is the result of chronic deficiencies of tumour oxygen supply as the result of long diffusion distance between tumour vessels, steep longitudinal pO₂ gradient along the vascular tree, blood viscosity and chaotic geometry of vascular network (Thomlinson and Gray 1955, Dewhirst *et al* 1999, Secomb *et al* 1998). In addition, acute hypoxia may also develop in tumour as the result of transient changes in oxygen delivery, oxygen consumption or both (Dewhirst 1998). Although changes in oxygen consumption cannot be ruled out, most previous studies have attributed the changes in local pO₂ primarily to alterations in oxygen supply. The commonly held view has been that acute hypoxia results primarily from vascular stasis. However, the low incidence of total vascular stasis (5%) suggests that this is not likely to be a major cause for transient hypoxia in tumours (Chaplin *et al* 1986, Dewhirst *et al* 1996). In contrast, microregional blood instabilities are a rather common phenomenon. The temporal instability in tumour red cell flux has been shown to be enough to cause transient oxygen deficiency in tumours (Kimura *et al* 1996). Several factors may contribute to flow fluctuations, including arteriolar vasomotion (Intaglietta *et al* 1977, Dewhirst *et al* 1996), rapid vascular modelling (Patan *et al* 1996) and other haemodynamic effects such as nonlinear flow properties of blood, non-uniform axial distribution of red blood cells within the vessel or disproportionate cell partitioning at bifurcations (Kiani *et al* 1994). Alternatively, it has been suggested recently in a mathematical model that the high interstitial fluid pressure and the high permeability of tumour vessels could explain the temporal heterogeneities of tumour blood flow observed *in vivo* (Mollica *et al* 2003).

It has become evident that acute hypoxia in solid tumours is not just a mechanistic curiosity but has significant therapeutical implications, causing resistance to radiation therapy (Chaplin *et al* 1987, Rofstad and Maseide 1999), contributing to tumour progression and

promoting the development of metastatic disease (Cairns *et al* 2001). Moreover, transient blood flow alterations may also impact critically on the delivery of chemotherapeutic agents and on the cellular responsiveness to these agents (Durand 2001).

Investigations of periodic changes in tumour microregional blood flow have so far been performed using intravital microscopy (Intaglietta *et al* 1977, Dewhirst *et al* 1996, Jain *et al* 2002), histologically based 'mismatch' techniques (Trotter *et al* 1989) and laser Doppler flowmetry (Chaplin and Hill 1995, Braun *et al* 1999). Measurements of temporal heterogeneity in pO₂ have been performed by using recessed tip oxygen microelectrode devices (Dewhirst *et al* 1996, Kimura *et al* 1996, Braun *et al* 1999) and, more recently, by using the OxyLite fibre-optic oxygen-sensing probe (Brurberg *et al* 2003, 2004). While the above methods have proved effective at uncovering the phenomenon of acute hypoxia, they are invasive or limited by a lack of spatial information and/or real-time data acquisition. Magnetic resonance imaging, on the other hand, is non-invasive and allows repeated measurements. Furthermore, T2*-weighted GRE images have proved useful for monitoring changes in tumour oxygenation and/or perfusion during therapy (Robinson *et al* 1997, Jordan *et al* 2000, Baudelet and Gallez 2002). The technique uses the endogenous contrast agent deoxyhaemoglobin as a source of contrast (blood oxygen level dependent or BOLD effect) (Ogawa *et al* 1990), and can also be sensitive to the 'inflow' effect (Howe *et al* 2001). On the basis of this T2*-weighted GRE technique's high temporal resolution, high spatial resolution and sensitivity to changes in blood flow and deoxyhaemoglobin content, we hypothesized that this technique may provide a useful means to enable non-invasive imaging of spontaneous blood flow fluctuations in tumours associated with acute hypoxia.

In the present study, we show that T2*-weighted GRE MRI, combined with suitable data treatment, is able to detect and to map localized, spontaneous temporal heterogeneity in signal intensity in intramuscularly implanted FSa fibrosarcoma murine tumours. First, a description of the MR signal fluctuations in terms of cycle time and spatial extent is provided. Next, we looked at whether scanner noise could contribute to generate these signal fluctuations, which would discredit the present method. We also examined whether such fluctuations could be ascribed to a systemic effect by analysing signal fluctuations acquired simultaneously from both tumour and contralateral muscle tissue. Next, to address the possible correlation between the T2*-weighted GRE spontaneous fluctuations and the acute hypoxia phenomenon, we examined the effects of some pharmacological agents, known to counteract acute hypoxia, on the fluctuation rate. Furthermore, we also performed multiple GRE MRI to track dynamic changes in T2* rather than changes in signal intensity (SI). Measurement of T2* relaxation times allows to monitoring of changes in the magnetic susceptibility, which depends more directly on changes in the oxyHb/deoxyHb ratio, thus avoiding the confounding effects of inflow and oxygenation (Lebon *et al* 1998). We also investigated whether fluctuations in T2*-weighted signal show an echo-time dependency, which is typical for physiological noise (Krüger and Glover 2001).

Finally, we performed dynamic contrast-enhanced MRI (DCE MRI), subsequent to the T2*-weighted GRE imaging, to answer the following questions: (i) Do the GRE fluctuations occur in actively perfused vasculature? (ii) Do the GRE fluctuations occur preferentially in neo-angiogenic vessels, characterized by highly permeable walls? As stated before, the high permeability of neo-vessels could make them very prone to fluctuations in blood flow (Mollica *et al* 2003). The DCE imaging was carried out using a rapid clearance blood pool agent, P792 (Port *et al* 2001). The study of the leakage of the MRI contrast agent from tumour vessels offers a means of assessing microvessel permeability, which is related to the early phase of the angiogenic process. After the imaging studies were completed, tumours were excised for histological examination.

Materials and methods

Mice and tumour model

Syngeneic FSa fibrosarcomas (Milas *et al* 1974) were inoculated into the hind leg muscle of male C3H/HeOulco mice. Mice were imaged when tumours were 10 mm in diameter (20 days later). Anaesthesia was provided by 1% isoflurane in air, administered with a facemask. The anaesthetized mice were secured using an adhesive tape to prevent any movement artefacts. A catheter was implanted intraperitoneally (i.p.) or intravenously (i.v.) to allow drug administration, and the mice were placed inside the magnet. Warm air was flushed into the magnet in order to maintain normothermia. Tumour temperature was monitored independently in three mice using an inserted thermocouple. No temperature fluctuations were observed during 2 h of monitoring under full experimental conditions (anaesthesia and MRI).

Imaging

MRI was performed with a 4.7 T (200 MHz, ^1H), 40 cm inner diameter bore system (Bruker Biospec, Ettlingen, Germany). T2-weighted anatomical images were acquired using a fast spin echo sequence (repetition time (TR) = 3 s, effective echo time (TE) = 63 ms). A single, 1.3 mm thick slice passing through the tumour centre was localized and imaged using a GRE sequence.

T2-weighted GRE MRI*

A surface coil, 2 cm in diameter, was used for radiofrequency transmission and reception. The T2*-weighted GRE sequence used the following parameters: TR = 200 ms, TE = 25 ms, flip angle = 45° , 12.5 kHz receiver bandwidth, 64 phase and frequency encode steps, 3 cm field of view, resulting in an in-plane resolution of $470\ \mu\text{m}$ and an acquisition time of 12.8 s. A run of 140 scans was acquired per 30 min time period.

A birdcage radiofrequency coil with an inner diameter of 70 mm was also used to image both tumour-bearing leg and contralateral muscle simultaneously. In this case, the T2*-weighted GRE sequence used the same parameters as described but, in order to maintain the same spatial resolution, the matrix size was kept 128×128 with FOV = 6 cm, which resulted in a doubled acquisition time (25.6 s). A run of 140 scans was therefore acquired per 1 h time period. Viewing the series of images in cine mode ensured absence of disturbing motion.

Multiple GRE MRI

A six-echo multi-GRE sequence was also used for the calculation of T2* maps. MR parameters were TR = 200 ms, TE = 6.1 ms, echo spacing = 6.02 ms, matrix size = 128×128 and FOV = 6 cm. The acquisition time was 25.6 s. Multi-GRE images were acquired continuously for 1 h. An image shift was observed between odd and even echoes. Therefore, only images at odd echoes were retained for the fit to a monoexponential decay function.

GRE fluctuation analysis

All MRI data were processed off-line using an in-house program written using IDLTM (Interactive Data Language, RSI, Boulder, CO) development software running on a PC. The aim of the analysis was to determine if temporal signals were significantly different from

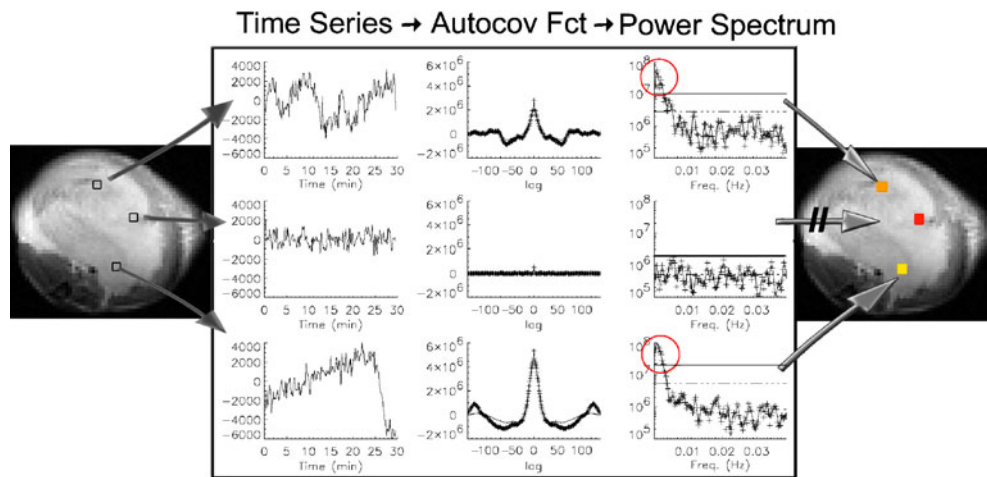


Figure 1. Illustration of the data processing. Left column: three types of T2*-weighted signal fluctuations (top to bottom) for representative voxels within a tumour (sampling time: 30 min): truly fluctuating voxels (TFV), not significantly fluctuating voxels (NFV) and voxels with signal drop (SDV). While some voxels showed random signal (middle), others showed structured time series (voxels above and below). Centre column: autocovariance plots. Maximum coefficient is found at zero lag, which is the variance of the signal. For random signals, the autocovariance function rapidly converges to zero as lag increases (middle). Autocovariance coefficients (+) are weighted (solid line) using a Bartlett window. Right column: power spectral density estimate (raw (+) and smoothed (solid line) power coefficients). PSD is yielded by the Fourier transformation of the weighted autocovariance function. Each smoothed power coefficient is tested for significance. The horizontal solid line represents the upper limit of a 99.99% confidence interval assuming Gaussian and white data. The dotted line represents the variance of the time series. For voxels above and below, significant coefficients are found at low frequencies (<0.056 Hz, i.e., <1 cycle/3 min) (see red circles). A map with the fluctuating zones is created; the colour scale reflects the variance of the signal, which is related to the magnitude of fluctuations.

Gaussian-distributed white noise. For this purpose a power spectrum analysis was performed (see details in Baudelet and Gallez (2003)). Briefly, an operator-defined region of interest encompassing the tumour was analysed on a voxel-by-voxel basis. The linear trends of the time series were removed using a regression procedure. The subtraction of the estimated linear trends (i.e., the regression line) from the raw temporal signal generated corrected time series with the mean signal intensity of zero. The windowed autocovariance functions of the corrected time series were then calculated (see figure 1). The Fourier transformation of the windowed autocovariance function yielded the power spectral density (PSD) estimate (Proakis and Manolakis 1988). The set of discrete frequencies ranged from 0.04 to 0.000 56 Hz (or from 0.02 to 0.000 28 Hz using the birdcage coil because of the doubled acquisition time). To obtain a more reliable estimate of the spectrum, the power coefficients were smoothed by a rectangular moving average window of width 3. Finally, the hypothesis that the data sequence came from Gaussian white noise was tested using a chi-square test for each smoothed power coefficient. The smoothed power coefficient ($\bar{\Psi}_{ij}$, where ij is the voxel location) at frequency f was considered significant when

$$[\bar{\Psi}_{ij}(f)] > \sigma^2 \frac{\chi^2(\alpha, \nu)}{\nu} \quad (1)$$

where σ^2 is the variance of the corrected time series, $\chi^2(\alpha, \nu)$ is the chi-square value for a given significance level α (0.001), $\nu = 6$ is the degrees of freedom associated with the rectangular smoothing window. For seven mice (control group), data were pooled from

all tumour voxels, and analysed for statistically significant fluctuation frequencies. A resulting histogram showed that power coefficients from a low-frequency band ranging up to 0.0056 Hz (i.e., <1 cycle/30 min to 1 cycle/3 min) were typically significant. Consequently, a voxel was termed 'fluctuating' when at least three smoothed power coefficients in this frequency range were found to be significant. The percentage of fluctuating voxels during a defined lapse of time (typically 30 min or 1 h) inside the region of interest was calculated as the number of fluctuating voxels divided by the total number of tumour voxels. Fluctuating voxels were overlaid on anatomical images in order to visualize the spatial distribution of the fluctuations. A colour scale reflects the variance of the sampled signal, which is related to the magnitude of the fluctuations (smallest values are red and largest values are yellow). The minimum (maximum) value of the scale is the minimum (maximum) square root variance value observed in the data set, and the scale is linear. Three-dimensional graphs (spatial coordinates and time) showing the original time course of signal intensity for the selected region were also created. The intensity scaling of each individual time series was not forced to prevent the relative flattening of the signals. A box was used to mark the fluctuating voxels. For these voxels, smoothed time series (moving average of width 3) were displayed to make trends clearer.

In addition, a classification of the spatio-temporal data was performed using a K-means cluster analysis (Baudalet and Gallez 2003). Voxels were grouped into three different categories according to the type of observed T2*-weighted GRE signal fluctuations: (i) not significantly fluctuating voxels (NFV), (ii) truly fluctuating voxels (TFV) and (iii) voxels with signal drop (SDV) (see figure 1).

To compare muscle and tumour fluctuations in terms of frequencies, we pooled data from seven mice from which tumour and muscle were imaged simultaneously. On a voxel-by-voxel basis, time-series data were subjected to the power spectrum analysis and all statistically significant frequencies were collected for both tissues. The frequency distribution of these significant peak frequencies was computed.

Pharmacological treatment

A group of mice ($n = 4$) were used to compare live and post-mortem fluctuations. After an initial 30 min of imaging, a pentobarbital overdose was administered for euthanasia. Consecutive 30 min windows were acquired until signal stabilization.

To investigate the pharmacological modulation of signal fluctuations, mice were initially imaged for 30 min. Inspired isoflurane was then temporarily increased to 2% for 2 min during drug injection to prevent animal movement (thereafter reset to 1%). After drug administration, images were acquired for another 90 min (=3 runs of 30 min). For the first treatment ($n = 6$), air delivery was permanently replaced by carbogen (95% O₂, 5% CO₂) and nicotinamide (Sigma-Aldrich, Bornem, Belgium) was administered i.p. (200 μ l, 500 mg kg⁻¹). In the second group ($n = 7$), pentoxifylline (Sigma-Aldrich, Bornem, Belgium) was administered i.p. (200 μ l, 50 mg kg⁻¹). In the third group ($n = 8$), flunarizine (Sigma-Aldrich, Bornem, Belgium) was administered i.p. (200 μ l, 5 mg kg⁻¹, dissolved in hydroxypropyl beta-cyclodextrin/0.9% NaCl solution, 5% W/V). In the control group ($n = 7$), saline was administered i.p. (200 μ l, 0.9% NaCl).

DCE MRI

In a complementary study ($n = 7$), dynamic contrast-enhanced MRI was performed, immediately following the T2*-weighted GRE MRI without removing the mouse from the

magnet. Two slices were selected for the dynamic contrast-enhanced study: one was centred on the kidneys and the other was positioned on the tumour, at the same location as for the GRE imaging. T1-weighted gradient-recalled echo images were obtained with the following parameters: TR = 40 ms, TE = 4.9 ms, 1.6 mm slice thickness, flip angle = 90°, matrix = 64 × 64, FOV = 6 cm, 25 kHz receiver bandwidth, resulting in an acquisition time of 2.56 s/scan. The contrast agent used was a rapid-clearance blood pool agent, P792 (Vistarem®, Laboratoire Guerbet, Aulnay sous Bois, France). P792 (mw: 6.47 kDa) is a monogadolinium macrocyclic compound based on a Gd-DOTA structure substituted by hydrophilic (dextran) arms. Its R1 relaxivity in 37 °C HSA, 4% at 4.7 T is 9.0 mM⁻¹ s⁻¹ (data communicated by Guerbet). P792 was injected at dose of 0.042 mmol Gd kg⁻¹ as recommended by the company and published studies (Fan *et al* 2004). The DCE study was performed using the following protocol. After 12 baseline images had been acquired, P792 was administered intravenously within 2 s (50 µl/40 g mouse) and the enhancement kinetics were continuously monitored for 8 min (200 total scans). In this way, the signal intensity curve was sampled often enough to track the fast rise in tissue enhancement for viable tumour following bolus arrival. Immediately after this, a slower DCE data set was acquired to monitor the washout of the contrast agent. For this second set, 60 scans were acquired at a temporal resolution of 60 s (1 h total).

Kinetic analysis

DCE MRI raw data were zero-filled and 2D Fourier transformed, resulting in an in-plane resolution of 128 × 128. An operator-defined region of interest encompassing the tumour was analysed on a voxel-by-voxel basis to obtain parametric maps. Voxels showing either no signal enhancement or linear increase of SI were excluded from the analysis. This was achieved by identifying voxels with statistically significant variations in T1-weighted signal intensity using the power spectrum analysis. Using cluster analysis, voxels for which typical signal enhancement curve was observed were then selected for the pharmacokinetic (Baudalet and Gallez 2003).

Contrast agent concentration as a function of time after P792 injection ($C(t)$) was estimated by comparing the tumour signal intensity as a function of time ($S(t)$) with the signal intensity in a reference tissue (muscle) with known T1 (Fan *et al* 2004). With the approximation that signal intensity changes linearly as a function of contrast media concentration (T1-weighted sequence, short TE, TR ≪ T1), then

$$C(t) = \frac{1}{R1 T1_{(\text{muscle})}} \frac{S(t) - S(0)}{S_{\text{muscle}}(0)} \quad (2)$$

where R1 is the longitudinal relaxivity of the contrast agent (assumed to be equal to that in HSA 4%) and the T1 of muscle is assumed to be 900 ms. The tracer concentration changes were fitted to a two-compartment pharmacokinetic model (Tofts 1997, Tofts *et al* 1999). In the model, the contribution of the tracer in the blood plasma to the total tissue concentration is included (negligible in blood–brain barrier lesion but often significant in tumours) and different permeability constants for flux into and out the extracellular extracellular space (EES) are allowed. The model assumes that the tracer is well mixed throughout the compartments (tumour regions with high interstitial fluid pressure might not meet this condition) and that there is a fast exchange of all mobile ¹H within the tissue. The model also assumes that the increase in T1 relaxation rate is proportional to the concentration of the tracer.

The equation describing the tissue concentration as a function of time is

$$C(t > t_0) = K_{\text{in}}^{\text{Trans}} A_0 \frac{\exp\left(-\frac{K_{\text{out}}^{\text{Trans}}}{v_e} t\right) - \exp(-k_1 t)}{k_1 - \frac{K_{\text{out}}^{\text{Trans}}}{v_e}} + v_p A_0 \exp(-k_1 t) \quad (3)$$

where $K_{\text{in}}^{\text{Trans}}$ is the influx volume transfer constant (into EES from plasma), $K_{\text{out}}^{\text{Trans}}$ is the efflux volume transfer constant (from EES back to plasma), v_e is the volume of EES per unit volume of tissue and v_p is the blood plasma volume per unit volume of tissue. $K_{\text{out}}^{\text{Trans}}$ and v_e cannot be estimated separately, so only k_{ep} , the ratio $K_{\text{out}}^{\text{Trans}}/v_e$, is reported. k_{ep} is the fractional rate of efflux from the interstitial space back to the blood. The constants used in the fitting are the maximum concentration of P792 in the plasma (A_0), the blood decay rate (k_1) and the time to the maximum tracer plasma concentration t_0 . It is assumed that the rapid enhancement phase (from $t = 0$ to t_0) is primarily due to intravascular contrast media during the first pass of the contrast media bolus, while the slower phase is due to leakage into the extracellular space. A universal t_0 time value was estimated for each mouse from the kidney data. Additionally, the decay rate of the contrast agent in the blood stream was estimated from the enhancement kinetics in one or two selected renal cortex voxels showing early and large [P792] signal enhancement, presumably reflecting pronounced arterial perfusion. A monoexponential function was fit to the [P792] kidney.

Fitting was performed using a Levenberg–Marquardt nonlinear least-squares procedure. Parametric images were computed and only the statistically significant parameter estimates were displayed. Statistical significance for v_p or $K_{\text{in}}^{\text{Trans}}$ identified ‘perfused’ voxels that displayed the typical signal curve enhancement after injection of the contrast agent.

Histological analysis

Immediately after DCE MRI session, animals were sacrificed by cervical dislocation. Tumours were resected, fixed in 10% buffered formalin, processed in order to obtain paraffin sections in the plane of the MR images and then stained with haematoxylin and eosin (H&E). Juxtaposed fields were photographed by a digital camera (Camedia 4040, Olympus Optical Co. Ltd, Tokyo, Japan) mounted on a BX60 Olympus microscope equipped with a $2\times$ magnification lens. A global image containing all the individually photographed fields was reconstructed using a ‘multiple images association’ function in an image analysis software program (DP Soft Analysis, Soft Imaging System, GmbH, Münster, Germany).

Results

Description of GRE signal fluctuations

Observing the behaviour of individual voxels over time provides direct information on the temporal and spatial fluctuation patterns inside a tumour. While some voxels showed independent temporal fluctuations, others showed synchronized temporal patterns (see figure 2). Typically, fluctuating voxels could be classified into two types: (a) truly fluctuating (TFV), i.e., showing sequential signal increase and decrease, as observed in isolated voxels, and (b) voxels with decreasing time series (SDV). For SDV voxels, we observed a profound drop in signal intensity with no subsequent recovery. This primarily involved clusters of neighbouring voxels (see figure 2).

When examining the spatial extent of GRE signal fluctuations, we found zones of spontaneous fluctuations that occupied up to 60% of the tumour area, with an average value of $33 \pm 4\%$ (mean \pm SEM). We also found evidence of temporal changes in areas within

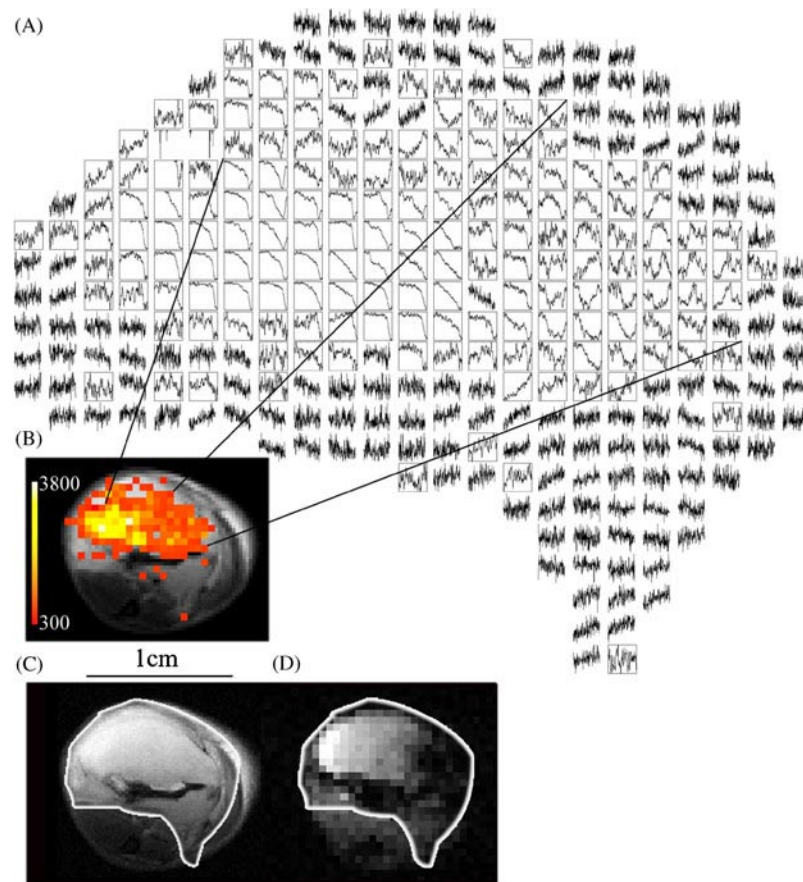


Figure 2. Fluctuating voxels and time course of signal intensity (SI). (A) Voxel-by-voxel plots of time course of SI. Boxes indicate voxels that were found to fluctuate on the basis of the spectral analysis. (B) Fluctuating map. Fluctuating voxels are located on the corresponding anatomical image. (C) T2-weighted anatomical image. (D) T2*-weighted image. The shape of the analysed tumour area is plotted on C and D. Different patterns of fluctuations are observed. They are classified into two types: truly fluctuating voxels (TFV) and voxels with signal drop (SDV). TFV are observed in isolated voxels and show poor correlation. In comparison, SDV concerned clusters of neighbouring voxels.

tumours showing spontaneous GRE signal fluctuations. When three sequential runs of 30 min imaging were analysed, a comparison of spatial coordinates of the fluctuating voxels revealed that $13 \pm 4\%$ of tumour voxels fluctuated in three out of three periods (III), $23 \pm 3\%$ in two out of three periods (II) and $31 \pm 3\%$ in just one 30 min period (I) (mean \pm SEM). The total for the three cited categories ($67 \pm 5\%$) represented the part of the tumour that exhibited fluctuations, and the remaining percentage ($33 \pm 5\%$) reflected the part of the tumour that did not experience fluctuations. Overall, this indicated that while some voxels were fluctuating at one time point, they were silent at other times ($p < 0.05$ when comparing I and III).

Distinction made between physiological noise and scanner instabilities

Signal fluctuations were compared in live versus deceased tumour-bearing mice. Utilizing the same mouse, but post-mortem, provided the ideal control. The physiological changes in

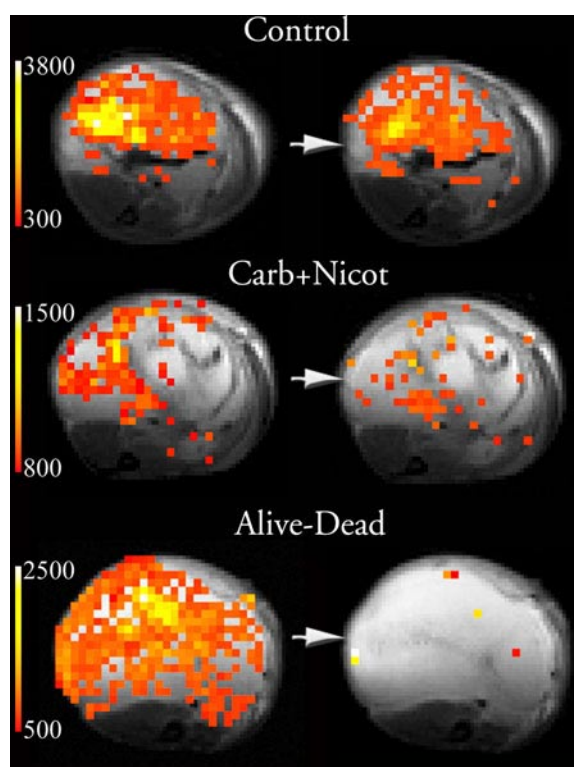


Figure 3. Illustration of the effects of different treatments on the number of fluctuating voxels inside the tumour (data come from three different animals). Each map represents the fluctuating zones over a 30 min sampling period (paired maps have the same colour scaling). Upper: control mouse. Centre: mouse pre and [30 min to 1 h] post carbogen breathing and nicotinamide administration. Note the decrease in the number of fluctuating voxels. Lower: before and [2 to 2.5 h] after death. Note the near complete cessation of fluctuations.

blood flow and pO_2 are expected to stop very soon after death. However, signal fluctuations continued to occur for up to 2 h after sacrifice, when the signals eventually stabilized. At this point, the proportion of fluctuating voxels was very small: deceased $2 \pm 1\%$ versus live $34 \pm 9\%$ (mean \pm SEM, paired t test, $p < 0.05$), indicating that the contribution of system imperfections to the observed fluctuations is almost negligible (see figure 3).

Response to treatments

During the first 30 min post drug administration, a general increase in the number of fluctuations was observed (average increase of $22 \pm 5\%$, mean \pm SEM, over untreated) inside the tumour. The changes manifested themselves primarily as a rapid increase or decrease in signal intensity, followed by recovery or not, until eventual signal stabilization. However, a statistically significant decrease in the percentage of voxels undergoing fluctuations was found for the next 30 min sampling period (i.e., [30 min to 1 h] post-treatment) in mice treated with carbogen and nicotinamide (C + N) (see figures 3 and 4), and in those treated with flunarizine (FLU), when compared to control. In contrast, pentoxifylline (PTX) was found to be ineffective in this study (see figure 4).

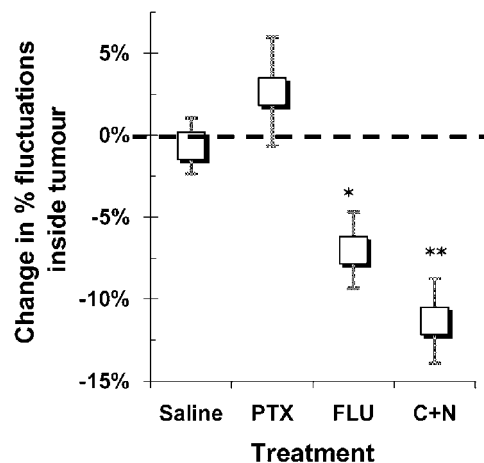


Figure 4. Effect of pharmacological interventions on T2*-weighted signal intensity fluctuations inside an FSa fibrosarcoma. Changes in the percentage of voxels exhibiting signal fluctuations inside tumour, observed [30 min to 1 h] post-treatment with pentoxifylline (PTX, $n = 7$), flunarizine (FLU, $n = 7$), combination of carbogen and nicotinamide (C + N, $n = 6$), or 0.9% NaCl (Saline, $n = 7$). Values are mean \pm SEM. * $p < 0.05$, ** $p < 0.01$.

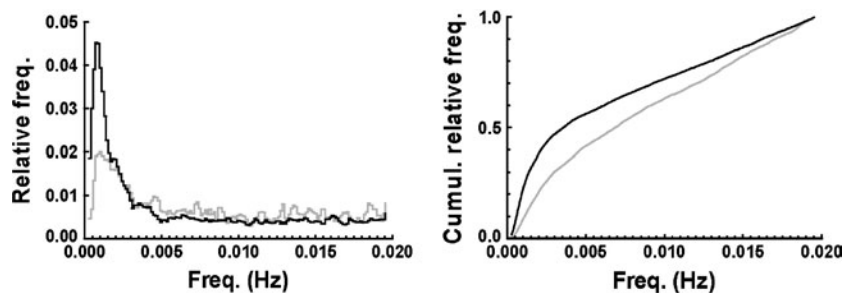


Figure 5. Frequency distribution of significant peak frequencies from power spectra of T2*-weighted signal fluctuations for tumour (black) and muscle (grey). Left: relative frequency distribution. For both tissues, most of the observed significant frequencies are in the low-frequency band (< 0.0055 Hz, i.e., < 1 cycle/3 min). Right: cumulative relative frequency distribution. More low-frequency fluctuations are observed in the tumour compared to the muscle (median has lower value for tumour).

Comparison of T2-weighted GRE fluctuations between tumour and contralateral muscle*

Analysis of the frequency distribution of the significant frequencies observed showed that both muscle and tumour tissues were subject to low fluctuation frequencies (see figure 5 (left)). However, tumour tissue was more subject to low-frequency fluctuations as reveals the cumulative frequency distribution (see figure 5 (right)). Median values for significant fluctuation frequencies were 0.0036 and 0.0070 Hz, respectively, for tumour and muscle ($p < 0.0001$). SDV voxels were not observed in the muscle, which might explain the relative higher frequency of fluctuations compared to the tumour.

Furthermore, we looked at whether muscle and tumour time series were correlated. Since the muscle could be considered as a homogeneous tissue, a region of interest (ROI) covering the muscle was defined and the average signal time course was measured. No significant temporal correlation was found between muscle and tumour fluctuations (see figure 6).

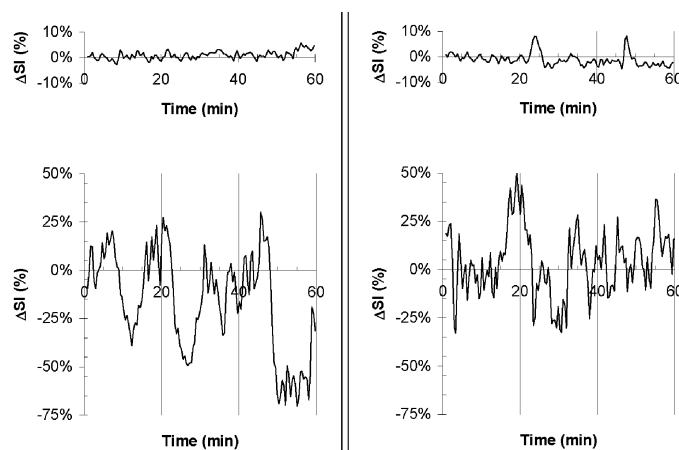


Figure 6. Comparison of average signal time course in the contralateral muscle (above) and single voxel signal in the tumour (below) for two mice (left and right). Muscle could also experience T2*-weighted signal fluctuations (two peaks were observed for the mouse data in the right-hand column). However, fluctuations in tumour signal intensity could not be explained by the changes observed in the muscle: either no apparent change is observed in the muscle tissue whereas it is present in the tumour (left) or both tissues experienced fluctuations that are not temporally correlated (right). *Note:* for the clarity of presentation, smoothed time curves are represented (moving average of width 3); this does not alter the information of fluctuations observed.

Multiple GRE imaging

The analysis of T2* parameter fluctuations (instead of T2*-weighted SI fluctuations) was somewhat problematic. Although T2* fluctuations were observed in tumour voxels (see figure 7A), fluctuation maps could not be generated reliably. For some points in the time series (in a given voxel), estimated T2* values were aberrant, due to the poor goodness of fit. This resulted in artefactual fluctuations. If aberrant values were discarded, then the length of the time series was not constant from one voxel to another for the PSD analysis. If aberrant values were replaced by a mean value, then the time series were artificially smoothed.

In addition, temporal data at three individual TE values (6, 18 and 30 ms) were submitted to PSD analysis to generate fluctuation maps. We observed that the per cent of significant SI fluctuations inside a tumour varies as a function of TE, with higher percentages at TE = 18 ms than at TE = 6 ms or TE = 30 ms (see figure 7B).

DCE MRI results and correlation with histological analysis

The two-compartment bidirectional pharmacokinetic model fitted adequately the DCE MRI data (see figure 8).

For some voxels, v_p was found to be non-significant whereas K_{in}^{Trans} , the rate of tracer accumulation in the interstitial space, was significant (see figures 9F and G). In these cases, the tumour region was not sufficiently well vascularized and the contribution of the blood volume was not large enough to be determined with a good precision. Correlation of maps of the T2*-weighted GRE spontaneous fluctuations with pharmacokinetic maps was investigated. Our results showed that the fluctuating regions were essentially located in areas with functional vasculature (regions where the contrast agent could flow in, i.e., characterized by significant values for v_p and/or K_{in}^{Trans}). About $71 \pm 6\%$ of voxels (mean \pm SEM) that present 'true fluctuations' (TFV) were perfused at the time DCE was performed (see figures 9D and F, G).

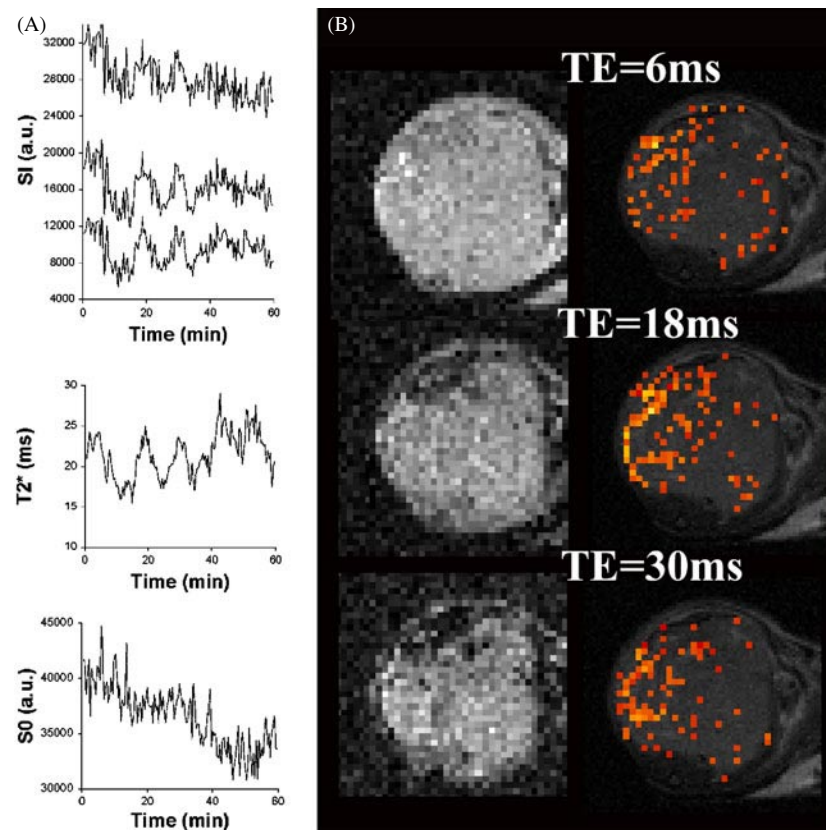


Figure 7. Dependence of signal intensity (SI) fluctuations on echo time. (A) Plot of evolution of SI at increasing echo times using multiple GRE imaging. SI fluctuations were increasingly visible as a function of TE, causing T2* (but not S0, the estimated signal at TE = 0 ms), to fluctuate. (B) Left column: GRE images, right column: maps of significant signal fluctuations at each individual (TE) Number of tumour voxels with significant SI fluctuations was lower at TE = 6 ms and 30 ms than at TE = 18 ms.

H&E stained sections, at locations comparable to the MR slices, showed that perfused regions corresponded to viable tumour with no evidence of massive necrosis (see figure 9I). On the other hand, only $42 \pm 8\%$ (mean \pm SEM, $p < 0.05$) of voxels with ‘signal drop’ (SDV) experienced a contrast agent flow, indicating a significantly worse perfusion status than TFV at the end of the T2*-weighted GRE imaging (see figures 9E and F, G). Histological section showed high vessel density in the regions associated with a darkening process (see figures 9I and A, B). Tumour vessels appeared dilated, accompanied or not by extravasation of erythrocytes (see figure 9J).

Pharmacokinetic parameters for fluctuating (TFV) and non-fluctuating voxels (NFV) are summarized in table 1. Only perfused TFV and NFV are compared. According to the pooled results, on average, TFV yielded lower values for v_p , and higher values for K_{in}^{Trans} and k_{ep} compared with NFV. In three tumours, K_{in}^{Trans} was found to be significantly higher for TFV than NFV. A high K_{in}^{Trans} value was associated in mouse 3 with a lower k_{ep} and in mouse 2, with a higher k_{ep} . Apparent v_e could be estimated if we assumed that both (in and out) apparent permeabilities are the same (in which case $v_e = K_{in}^{Trans}/k_{ep}$). Mean v_e values

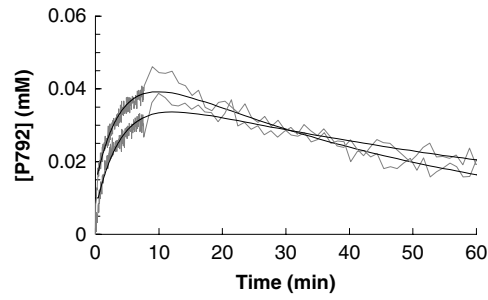


Figure 8. Fit of the model to dynamic curves of the contrast medium concentration to derive the parameters v_p , K_{in}^{Trans} and k_{ep} . Data are whole tumour signal for two individual tumours, after intravenous injection of P792 contrast agent (P792 blood kinetics were similar for both mice, with $A_0 = 0.41$ versus 0.41 mM and, $k_1 = 0.064$ versus 0.060 min^{-1}). Estimated parameters obtained from the fitting are (value \pm SE): curve 1, v_p : 0.0164 ± 0.0009 , K_{in}^{Trans} : 0.0246 ± 0.0002 min^{-1} , k_{ep} : 0.0113 ± 0.0004 min^{-1} ; curve 2, v_p : 0.0336 ± 0.0001 , K_{in}^{Trans} : 0.0288 ± 0.0002 min^{-1} , k_{ep} : 0.0189 ± 0.0004 min^{-1} . v_p is the apparent fractional plasma volume (determines the rapid enhancement phase), K_{in}^{Trans} is the influx volume transfer constant (proportional to the contrast uptake rate) and k_{ep} is the fractional rate of efflux from the EES back to blood.

Table 1. Comparison of v_p , K_{in}^{Trans} and k_{ep} parameters for truly fluctuating (TFV) and non-fluctuating voxels (NFV). Individual and pooled data.

Mouse	v_p		K_{in}^{Trans} (min^{-1})		k_{ep} (min^{-1})				
	TFV	NFV	TFV	NFV	TFV	NFV			
1	0.036 ± 0.004	0.055 ± 0.003	**	0.033 ± 0.002	0.037 ± 0.001	<i>ns</i>	0.045 ± 0.009	0.046 ± 0.005	<i>ns</i>
2	0.055 ± 0.006	0.048 ± 0.004	<i>ns</i>	0.059 ± 0.008	0.036 ± 0.004	*	0.162 ± 0.020	0.112 ± 0.012	*
3	0.016 ± 0.002	0.025 ± 0.002	**	0.025 ± 0.001	0.018 ± 0.001	***	0.042 ± 0.005	0.080 ± 0.012	**
4	0.047 ± 0.004	0.046 ± 0.002	<i>ns</i>	0.021 ± 0.002	0.020 ± 0.001	<i>ns</i>	0.146 ± 0.020	0.141 ± 0.012	<i>ns</i>
5	0.029 ± 0.006	0.048 ± 0.002	**	0.029 ± 0.004	0.027 ± 0.002	<i>ns</i>	0.166 ± 0.037	0.133 ± 0.012	<i>ns</i>
6	0.056 ± 0.003	0.056 ± 0.002	<i>ns</i>	0.027 ± 0.002	0.024 ± 0.001	<i>ns</i>	0.120 ± 0.014	0.094 ± 0.008	<i>ns</i>
7	0.058 ± 0.004	0.050 ± 0.003	<i>ns</i>	0.038 ± 0.001	0.029 ± 0.001	***	0.070 ± 0.007	0.065 ± 0.007	<i>ns</i>
Pooled	0.042 ± 0.006	0.047 ± 0.004	<i>ns</i>	0.033 ± 0.005	0.027 ± 0.003	<i>ns</i>	0.108 ± 0.022	0.096 ± 0.013	<i>ns</i>

Values are mean \pm SEM, *** $p < 0.001$; ** $p < 0.01$; * $p < 0.05$; *ns*: $p > 0.05$. Student's unpaired (individual) or paired (pooled data) *t* test.

for TFV and NFV are similar (respectively 0.40 ± 0.09 , 0.34 ± 0.09 , mean \pm SEM, *ns*). TFV in mouse 3 exhibited typically high v_e (three times higher) compared with NFV. This could explain why k_{ep} for TFV is lower than k_{ep} for NFV.

Discussion

Cycle time of the $T2^*$ -weighted GRE fluctuations

The observed cycle times of the spontaneous $T2^*$ -weighted GRE fluctuations in control tumour data (from <1 cycle/30 min to 1 cycle/3 min) are similar to cycle times of fluctuations in tumour blood flow and oxygen as reported previously by using alternative techniques. For example, a periodicity of 2–3 min was found for fluctuations in microvascular flow in 'sandwich' tumours (Intaglietta *et al* 1977, Dewhirst *et al* 1996). Trotter *et al* reported a tumour blood vessel closure duration of at least 5 min using fluorescent dyes techniques (Trotter *et al* 1989). Interestingly, blood flow fluctuations with extremely low cycle times,

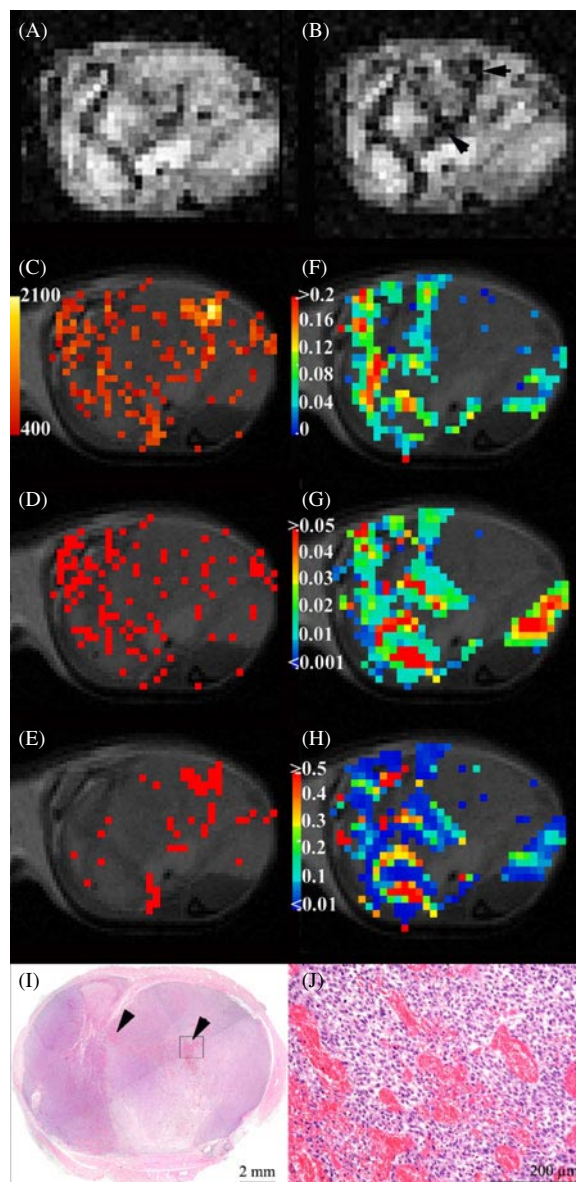


Figure 9. (A, B) T2*-weighted images at the beginning (A) and at the end (B) of the T2*-weighted GRE imaging. Note the darkening in some tumour zones (arrows). (C) Fluctuation map. The fluctuating zones appear spatially organized. (D-E) Statistically significant signal fluctuations are classified into two types: TFV (D) and SDV (E). (F-H) Pharmacokinetic parameter maps. (F) v_p parameter map. For some voxels, v_p was not found to be significant, indicating no detectable vascular volume (not coloured). (G) K_{in}^{Trans} parameter map. A large part of the tumour core did not experience signal enhancement upon contrast agent injection. (H) k_{ep} parameter map. From these maps, it can be observed that the TFV (unlike SDV) are located mainly in zones with contrast enhancement (v_p and/or K_{in}^{Trans} significant). (I, J) Corresponding H&E histological section. (I) Viable areas are characterized by a high affinity for haematoxylin (pink/blue colour), and correspond to tumour zones with significant v_p and/or K_{in}^{Trans} . High vessel density was observed in regions becoming dark (SDV) in the T2*-weighted images (arrows). (J) Tumour vessels appeared large (hyperaemia, mean vessel diameter: 40–50 μm). Diffuse haemorrhage is also visible (extravasation of erythrocytes).

ranging from 10 to 60 min, have also been described (Dewhirst *et al* 1996). We also observed such low fluctuation frequency. A direct comparison of these studies is difficult, however, because of the difference in sampling volume of these techniques. Methods such as intravital microscopy, dye mismatch methods or recessed-tip micro electrodes employ measurements on the microvascular scale, which is substantially smaller than MRI voxels (in-plane resolution of 470 μm). The frequency behaviour of the GRE time-series fluctuations can be compared more easily with the frequency of the flow fluctuations measured by laser Doppler techniques. Indeed, the laser Doppler flow signal is typically integrated over a semi-hemisphere with a radius ranging from 200 μm to 1 mm, which is close to our MRI voxel sizes. Chaplin *et al* observed that the duration of erythrocyte flow change ranged from 6 to 45 min during a 1 h sampling period (Chaplin and Hill 1995), while Braun *et al* reported that almost all the spontaneous fluctuations in tumour blood flow occurred at very low frequencies ranging from 0.2 to 2 cycles min^{-1} (Braun *et al* 1999). These studies of the temporal heterogeneity in blood flow in tumours support our findings. Moreover, the temporal heterogeneity in the T2*-weighted GRE tumour fluctuations are similar to the frequency range of pO₂ fluctuations measured by microelectrodes and the OxyLite system. The comparison of the MRI data with the OxyLite system is very important, considering the similarity of the sampling volumes. Fourier analysis of the pO₂ traces measured by OxyLite probes fluctuated at frequencies lower than 1 cycle/10 min (Brurberg *et al* 2003, 2004). Using the OxyLite/OxyFlo system, we also found pO₂ and red cell flux fluctuations comparable to those observed in TFV in independent tumours (data not shown).

Distinction made between physiological noise and scanner instabilities

It has been reported that non-physiological artefacts in T2*-weighted signal intensity can be ascribed to thermal noise from scanner electronics or imperfections in RF gradient and shim subsystems (Smith *et al* 1999). By comparing the live and post-mortem fluctuations, we showed that the T2*-weighted GRE signal fluctuations did not originate from scanner imperfections. Indeed, 2 h post-mortem, a near complete cessation of fluctuations was observed. Another interpretation for this would be that scanner instabilities contribute to fluctuations until the water signal linewidth becomes so broad that sensitivity to these temporal variations is lost. This is not likely to occur. First, unexpectedly (with regards to what is occurring in the brain tissue), the average signal intensity in the tumour tissue increased post-mortem, suggesting an increase rather than a decrease in T2* (Ogawa *et al* 1990). Howe *et al* has reported similar observations when MNU tumours were imaged during 100% N₂ breathing until post-mortem (Howe *et al* 2001). An increase in T2* as much as that for 100% O₂ breathing, was observed. They interpreted the image changes as follows. Depending on the patency of the tumour blood vessels and the interstitial fluid pressure, vascular collapse can occur post-mortem, thereby reducing tissue deoxyHb concentration. Signal fluctuations observed during the first two hours after sacrifice were clearly not related to transient fluctuations of blood flow. Instead, shrinkage of the leg during the onset of rigor mortis could have generated signal fluctuations, essentially at tissue boundaries. Also, cytoarchitectural arrangement, and an overall increase in the available fluid space in the post-mortem situation due to oncosis (Van Cruchten and Van Den Broeck 2002) causing change in the apparent T2/T1 could produce change in SI.

MRI signal fluctuations could still originate from respiratory and cardiac noise, as has been demonstrated to occur in the brain (Windischberger *et al* 2002). At the sampling rate we employed (maximum observable frequency: 2.3 cycles min^{-1} or 0.039 Hz), the respiratory and cardiac peaks that might appear artefactually in the low-frequency range could not be

characterized (occurring at 2 and 8 Hz, respectively). To eliminate this effect, acquisitions with extremely fast sampling rates would be needed: image acquisition times less than 60 ms to resolve the cardiac fundamental frequency or less than 250 ms to resolve at least the respiratory peak. Alternatively, cardiac gating could provide a means to compensate for cardiac-related artefacts. Image acquisition could be triggered by a start pulse derived from an ECG lead or via a peripheral pulse oximeter. In standard GRE imaging, a single image line (k space) would be acquired in each cardiac cycle. This would imply that the current TR used in this study (200 ms) should be reduced to match the time between consecutive heartbeats (approx. 60 ms). This shortened TR would reduce the signal-to-noise ratio (SNR), which would have to be taken into account. Similarly, respiratory effects could be compensated via gating.

Although a contribution of respiratory or cardiac noise cannot be ruled out in the present study, it is very likely that the signal fluctuations were related primarily to the tumour physiology. First, T2*-weighted signal fluctuations in different regions of a tumour in general were temporally independent (see figure 2), suggesting that they were caused primarily by redistribution of the perfusion within the tumour rather than by cardiac and respiratory functions that cause quasiperiodic oscillation in the vascular system. Second, our results showed that some voxels affected by signal fluctuations at one time were not affected at another time. There is no reason why the contribution of the cardiac and respiratory functions to the T2*-weighted signal fluctuation would cease during a new acquisition run.

Issues in the detection of fluctuating voxels using PSD analysis

The rationalization for removing linear trends prior to calculating the autocovariance function was that a drift is a pattern of noise. However, this procedure can potentially suffer from certain limitations. The first limitation is that fairly linear time series changes associated with the physiological status of the tumour could not be differentiated from a linear baseline drift. We observed that the darkening process on T2*-weighted imaging of tumour was expressed either as a gradual linear signal loss or as a sudden significant signal intensity drop. During the data processing, the voxel was not considered as fluctuating for the former case, whereas it was for the latter case (SDV). Consequently, we may have underestimated the extent of spontaneous fluctuations, especially for SDV. The second limitation of removing linear trends is that it may introduce bipolar features into the time series that could appear as spurious frequency components following Fourier transform, thereby generating false positive results. However, when we investigated this, we found that the selected time series would also have been identified as fluctuating if no drift correction had been performed.

Tumour versus muscle fluctuations

In the muscle tissue, low-frequency T2*-weighted GRE fluctuations were also observed. These fluctuations appeared not to be temporally correlated to those arising in tumour tissue, which indicated that they were independent phenomena. This therefore discounted the possibility that an acute systemic effect, such as blood pressure change, could have produced signal fluctuations in the tumour. Low-frequency fluctuations in muscle blood flow and pO₂ have already been reported (Braun *et al* 1999). Braun *et al* noted that tumours exhibit more low-frequency blood flow activity than muscle, as we have also observed (Braun *et al* 1999). The greater low-frequency activity in T2*-weighted fluctuations in tumour might in part be due to the presence of voxel signal drop. In addition, the Braun group observed that the fluctuations in tumours had a higher magnitude than those in muscle. In our study, a comparison of muscle and tumour fluctuations in terms of magnitude would not be valid because of the qualitative nature of the technique and the different native T2 for both tissues.

Pharmacological modulation of tumour T2-weighted GRE fluctuations*

We investigated the ability of some treatments aimed at abolishing perfusion-limited hypoxia to modify the incidence of tumour T2*-weighted GRE fluctuations. Three treatments were tested in this study: (1) carbogen and nicotinamide, (2) flunarizine and (3) pentoxifylline. These drugs are known to enhance the radiation sensitivity of tumours and have been proposed as possible modifiers of acute hypoxia (Hill and Chaplin 1995, Bennewith and Durand 2001, Wood and Hirst 1988). Accelerated radiotherapy with nicotinamide and carbogen breathing is currently undergoing clinical testing (Kaanders *et al* 2002). Flunarizine, which is a calcium channel blocker, and pentoxifylline, which is a methylxanthine derivative, have both been known to decrease blood viscosity and increase tumour blood flow. In the present study, we saw evidence of a decrease in the incidence of fluctuations when tumours were treated with carbogen and nicotinamide or flunarizine, during the [30 min to 1 h] time window post drug administration. Immediately following the drug administration [0 min to 30 min], there is a general increase in the number of signal fluctuations. These early effects are consistent with the rapid modification of tumour blood flow/pO₂ by vasoactive agents (e.g., Jordan *et al* 2000, Baudalet and Gallez 2002). Additionally, we also previously reported that these signal changes could be highly heterogeneous in temporal behaviour with opposite patterns encountered in adjacent tumour locations (Baudalet and Gallez 2003). What is important in this part of the study is that the observed decreased incidence in signal intensity changes (i.e., >30 min after administration of the drug) further support the likelihood that the spontaneous fluctuations we detected are related to underlying tumour pathophysiological process, such as acute hypoxia. The absence of significant results with pentoxifylline could be explained by the short-lasting drug effect. Bennewith *et al*, using pentoxifylline at the same dosage, demonstrated that tumour blood flow increased within 15 min after administration and returned to control levels by 30 min (Bennewith and Durand 2001). A redistribution of the microregional perfusion was found to last at least 30 min, but there were no data available to evaluate a longer lasting effect. It might be worth modifying drug administration schedule (e.g., repeated injection) to increase the time window of the potential benefit of pentoxifylline on perfusion-limited hypoxia.

DCE MRI

The tumour microenvironment in which spontaneous T2*-weighted GRE fluctuations were occurring was characterized in terms of vessel functionality, vascularity and vessel permeability, by DCE MRI using P792, a rapid clearance blood pool agent. P792 leaks more slowly from blood vessels compared to Gd-DTPA, but its leakage rate is still much faster than albumin-Gd-DTPA (Fan *et al* 2004, Turetschek *et al* 2001). The pharmacokinetic model used for the interpretation of intermediate size tracer uptake was the Tofts model that was originally designed for Gd-DTPA kinetics (Tofts 1997). The extended version of the model includes contribution of tracer in the blood plasma (to estimate v_p) and accounts for different permeability of flux into and out the EES. Three parameters were extracted: v_p , K_{in}^{Trans} and k_{ep} . In this study we administered the tracer once only, at the end of T2*-weighted GRE MRI acquisition. Ideally, repeated administration of the tracer would have made it possible to probe the microenvironment of the tumour at different time points (e.g., before and after T2*-weighted GRE MRI). However, the long-lasting enhancement kinetics of the contrast agent necessarily limits the time interval between two measurements. Our results showed that TFV were predominantly located in regions with functional vessels, where a contrast agent could flow in. In contrast, fluctuations characterized by a signal drop appeared to occur in regions with no contrast enhancement. Lack of contrast enhancement would have resulted from either non-functional capillaries or non-vascularized regions. Histological sections indicated that

the capillaries for these regions were present but non-functional. Under the microscope, the vessels were densely populated but appeared dilated, which implied flow resistance and thus functional impairment. Vasodilatation and/or deoxygenation of vessels due to blood flow impairment could explain dramatic decreases in the signal intensity in T2*-weighted images because of the associated increase in deoxyhaemoglobin concentration.

We also investigated whether the pharmacokinetic parameters could differentiate regions demonstrating truly fluctuating GRE signals from those that were not fluctuating. In 3/7 tumours, TFV showed significantly higher K_{in}^{Trans} values than NFV, suggesting that transient fluctuations were occurring preferentially in neoangiogenic hypermeable vessels. While not always significant, this trend was observed in 6/7 mice. It should be noted that the transfer constant K^{trans} has several physiological interpretations, depending on the balance between capillary permeability and blood flow in the tissue of interest (Tofts 1997). If flux across the endothelium is permeability limited, K^{trans} is the permeability surface area product per unit volume of tissue. In this case, K^{trans} should be regarded as apparent permeability. In the case of flow limited condition (e.g. regions with high permeability or poor blood supply), K^{trans} would reflect blood plasma flow. There are two arguments for the permeability limited condition. First, although estimated K_{in}^{Trans} values were about five times greater than those reported in previous studies using P792 (Turetschek *et al* 2001, Pradel *et al* 2003), they were well below those that are obtained using Gd-DTPA, where K^{trans} values are greater than 1 min^{-1} (Taylor and Reddick 2000, Galbraith *et al* 2002). In addition, in the present analysis, K^{trans} values were not estimated for voxels showing linear enhancement, precisely to exclude regions with poor blood supply. On average, k_{ep} values were also higher for TFV than for NFV, while the volume of extravascular extracellular space did not vary between both types of voxels. This also indicated that transient fluctuations were occurring preferentially in neoangiogenic hypermeable vessels. TFV were also characterized by lower values for apparent fractional plasma volume. Possible reasons for this would be that the fractional blood volume was lower or that the haematocrit was higher (at given blood volume, plasma volume would be lower). Bhujwala *et al* reported that regions of high permeability were observed in regions with low vascular volume values (Bhujwala *et al* 2003).

The global statistical non-significance for differences in v_p , K_{in}^{Trans} and k_{ep} between TVF and NFV suggested that these factors alone could not explain the occurrence of the fluctuations. The causes of instability in microregional blood flow, which is thought to generate acute hypoxia, is still a matter of intense research. Important mechanisms other than the high permeability of neo-vessels have been suggested, such as arteriolar vasomotion (Intaglietta *et al* 1977, Dewhirst *et al* 1996), tortuous vascular architecture (Kiani *et al* 1994) and rapid vascular remodelling associated with microvascular growth (Patan *et al* 1996). Finally, it should be emphasized that our observations are only valid for low-frequency fluctuations. For example, high-frequency fluctuations associated with vasomotion (typically ranging from 1 to 15 cycles min^{-1}) cannot yet be studied using the MRI parameters that were used in the present work.

Dissecting T2-weighted GRE signal fluctuations*

What causes the observed signal fluctuations? The signal intensity (SI) of T2*-weighted GRE sequences are sensitive to changes in both deoxyhaemoglobin content (BOLD T2* contrast) and blood flow (inflow effect) (Howe *et al* 2001). Thus, for a more 'pure' measurement, it would be better to track the dynamic changes in T2* rather than changes in SI. Extraction of T2* relaxation times allows monitoring of changes in the magnetic susceptibility, which has a more direct dependence on changes in the oxyHb/deoxyHb ratio. Yet, from multiple

GRE data, we observed an echo-time dependency of the signal fluctuations, which is unique to physiological noise (Krüger and Glover 2001). The rationale for analysing the TE dependence of the percentage of voxels with significant fluctuations lies in the TE dependence of the BOLD contrast-to-noise ratio (maximum at $TE = T2^*$). As the TE approaches $T2^*$, BOLD fluctuations are increasingly visible against the background noise, making them more easily detected by the PSD analysis. In addition, we reported that the analysis of multiple GRE images to generate $T2^*$ parameter maps was not reliable. The SNR, which is critical for estimating $T2^*$, was insufficient when performing 'rapid' acquisition time imaging and voxel-by-voxel analysis. High spectral and spatial (HiSS) imaging MRI could be an alternative to improve the quality of functional information (Al-Hallaq *et al* 2002, 2003). Spectroscopic imaging allows highly accurate measurements of $T2^*$ and can distinguish between changes in $T1$ and $T2^*$. However, high spectral resolution results in loss of signal-to-noise ratio and increased image acquisition time. Further work will be required to compare conventional GRE and HiSS imaging in terms of their ability to detect physiological fluctuations of blood flow and oxygenation in tumours.

A change in $T2^*$ can reflect changes in several physiological parameters such as blood HbO_2 saturation, haematocrit, blood volume or blood flow. This property can be used to assess treatment designed to alter tumour oxygenation (Jordan *et al* 2000, Baudalet and Gallez 2002, Howe *et al* 2001), to monitor the rise in vessel density associated with angiogenesis (Abramovitch *et al* 1998), or to measure tumour vessel maturation (Neeman *et al* 2001). However, while the sensitivity of $T2^*$ -weighted GRE imaging to changes in tumour deoxyhaemoglobin concentration has been clearly demonstrated, the interpretation of the signal change in terms of the meaningful physiological parameter, tumour pO_2 change, is not straightforward. This is a potential limitation of the use of $T2^*$ -weighted MRI to assess acute hypoxia phenomena. Indeed, in the simplest case, signal changes are proportional to tumour pO_2 but changes are only of a qualitative nature (Baudalet and Gallez 2002). Additionally, changes in blood volume can counteract the effect of blood oxygenation change (Howe *et al* 2001). Alternatively, MRI techniques that can provide absolute quantification of pO_2 (e.g., ^{19}F NMRI, EPR imaging and Overhauser imaging) could be more relevant than $T2^*$ -weighted MRI to assess acute hypoxia phenomenon (Hunjan *et al* 2001, Krishna *et al* 2002). However, currently the temporal resolution of these other techniques is still limited.

Conclusion

Spontaneous $T2^*$ -weighted GRE fluctuations are very likely to be related to spontaneous fluctuations in blood flow and oxygenation associated with the pathophysiology of acute hypoxia in tumours, for the following reasons: (1) the fluctuations are independent of the scanner instability; (2) they show spatial and temporal heterogeneity over the tumour; (3) they are not correlated to the fluctuations occurring in the muscle tissue; (4) they are dampened by pharmacological agents known to modulate acute hypoxia in tumours; and (5) they are related to the hyperpermeability of blood vessels. The major advantage of this MRI technique lies in its capacity to provide simultaneously both temporal and detailed spatial information on spontaneous fluctuations throughout the tumour. The disadvantage is the complexity of signal interpretation in terms of its relation to pO_2 changes. As a method for studying the tumour microenvironment, $T2^*$ -weighted GRE MRI should be considered as complementary to established techniques such as intravital microscopy, which requires window chamber models, or histological methods, which are limited to only two time point measurements. Moreover, because of the non-invasive nature of MRI and the growing availability of MRI scanners operating at high magnetic fields, it seems likely that the method described could be

readily applied in the clinic. There, it could facilitate the study of acute hypoxia in tumours and speed the development of pharmacological treatments designed to modulate tumour hypoxia.

Acknowledgments

This work was supported by the Belgian National Fund for Scientific Research (grants 3.4560.00 and 7.4503.02) and the Fonds Joseph Maisin. The authors thank Mrs C Clorot (Guerbet Laboratories, Roissy, France) for providing P792. This work was presented in part at the 19th Annual Meeting of the ESMRMB, Cannes, 22–25 August 2002 and the ISMRM 11th Scientific Meeting, Toronto, 10–16 July 2003.

References

- Abramovitch R, Frenkiel D and Neeman M 1998 Analysis of subcutaneous angiogenesis by gradient echo magnetic resonance imaging *Magn. Reson. Med.* **39** 813–24
- Al-Hallaq H A, Fan X, Zamora M, River J N, Moulder J E and Karczmar G S 2002 Spectrally inhomogeneous BOLD contrast changes detected in rodent tumors with high spectral and spatial resolution MRI *NMR Biomed.* **15** 28–36
- Al-Hallaq H A, Zamora M A, Fish B L, Halpern H J, Moulder J E and Karczmar G S 2003 Using high spectral and spatial resolution bold MRI to choose the optimal oxygenating treatment for individual cancer patients *Adv. Exp. Med. Biol.* **530** 433–40
- Baudelet C and Gallez B 2002 How does blood oxygen level-dependent (BOLD) contrast correlate with oxygen partial pressure (pO₂) inside tumors? *Magn. Reson. Med.* **48** 980–6
- Baudelet C and Gallez B 2003 Cluster analysis of BOLD fMRI time series in tumors to study the heterogeneity of hemodynamic response to treatment *Magn. Reson. Med.* **49** 985–90
- Bennewith K L and Durand R E 2001 Drug-induced alterations in tumour perfusion yield increases in tumour cell radiosensitivity *Br. J. Cancer* **85** 1577–84
- Bhujwala Z M, Artemov D, Natarajan K, Solaiyappan M, Kollars P and Kristjansen P E 2003 Reduction of vascular and permeable regions in solid tumors detected by macromolecular contrast magnetic resonance imaging after treatment with antiangiogenic agent TNP-470 *Clin. Cancer Res.* **9** 355–62
- Braun R D, Lanzen J L and Dewhirst M W 1999 Fourier analysis of fluctuations of oxygen tension and blood flow in R3230Ac tumors and muscle in rats *Am. J. Physiol.* **277** H551–68
- Brurberg K G, Graff B A, Olsen D R and Rofstad E K 2004 Tumor-line specific pO₂ fluctuations in human melanoma xenografts *Int. J. Radiat. Oncol. Biol. Phys.* **58** 403–9
- Brurberg K G, Graff B A and Rofstad E K 2003 Temporal heterogeneity in oxygen tension in human melanoma xenografts *Br. J. Cancer* **89** 350–6
- Cairns R A, Kalliomaki T and Hill R P 2001 Acute (cyclic) hypoxia enhances spontaneous metastasis of KHT murine tumors *Cancer Res.* **61** 8903–8
- Chaplin D J, Durand R E and Olive P L 1986 Acute hypoxia in tumors: implications for modifiers of radiation effects *Int. J. Radiat. Oncol. Biol. Phys.* **12** 1279–82
- Chaplin D J and Hill S A 1995 Temporal heterogeneity in microregional erythrocyte flux in experimental solid tumours *Br. J. Cancer* **71** 1210–3
- Chaplin D J, Olive P L and Durand R E 1987 Intermittent blood flow in a murine tumor: radiobiological effects *Cancer Res.* **47** 597–601
- Dewhirst M W 1998 Concepts of oxygen transport at the microcirculatory level *Semin. Radiat. Oncol.* **8** 143–50
- Dewhirst M W, Kimura H, Rehmus S W, Braun R D, Papahadjopoulos D, Hong K and Secomb T W 1996 Microvascular studies on the origins of perfusion-limited hypoxia *Br. J. Cancer* **27** S247–51
- Dewhirst M W, Ong E T, Braun R D, Smith B, Klitzman B, Evans S M and Wilson D 1999 Quantification of longitudinal tissue pO₂ gradients in window chamber tumours: impact on tumour hypoxia *Br. J. Cancer* **79** 1717–22
- Durand R E 2001 Intermittent blood flow in solid tumours—an under-appreciated source of ‘drug resistance’ *Cancer Metastasis Rev.* **20** 57–61
- Fan X, Medved M, River J N, Zamora M, Corot C, Robert P, Bourrinet P, Lipton M, Culp R M and Karczmar G S 2004 New model for analysis of dynamic contrast-enhanced MRI data distinguishes metastatic from nonmetastatic transplanted rodent prostate tumors *Magn. Reson. Med.* **51** 487–94

- Galbraith S M, Lodge M A, Taylor N J, Rustin G J, Bentzen S, Stirling J J and Padhani A R 2002 Reproducibility of dynamic contrast-enhanced MRI in human muscle and tumours: comparison of quantitative and semi-quantitative analysis *NMR Biomed.* **15** 132–42
- Hill S A and Chaplin D J 1995 The effect of nicotinamide on microregional blood flow within tumours assessed using laser Doppler probes *Acta Oncol.* **34** 401–4
- Howe F A, Robinson S P, McIntyre D J, Stubbs M and Griffiths J R 2001 Issues in flow and oxygenation dependent contrast (FLOOD) imaging of tumours *NMR Biomed.* **14** 497–506
- Hunjan S, Zhao D, Constantinescu A, Hahn E W, Antich P P and Mason R P 2001 Tumor oximetry: demonstration of an enhanced dynamic mapping procedure using fluorine-19 echo planar magnetic resonance imaging in the Dunning prostate R3327-AT1 rat tumor *Int. J. Radiat. Oncol. Biol. Phys.* **49** 1097–108
- Intaglietta M, Myers R R, Gross J F and Reinhold H S 1977 Dynamics of microvascular flow in implanted mouse mammary tumours *Bibl. Anat.* **15** 273–6
- Jain R K, Munn L L and Fukumura D 2002 Dissecting tumour pathophysiology using intravital microscopy *Nature Rev. Cancer* **2** 266–76
- Jordan B F, Misson P, Demeure R, Baudelet C, Beghein N and Gallez B 2000 Changes in tumor oxygenation/perfusion induced by the no donor, isosorbide dinitrate, in comparison with carbogen: monitoring by EPR and MRI *Int. J. Radiat. Oncol. Biol. Phys.* **48** 565–70
- Kaanders J H, Bussink J and van der Kogel A J 2002 ARCON: a novel biology-based approach in radiotherapy *Lancet Oncol.* **3** 728–37
- Kiani M F, Pries A R, Hsu L L, Sarelius I H and Cokelet G R 1994 Fluctuations in microvascular blood flow parameters caused by hemodynamic mechanisms *Am. J. Physiol.* **266** H1822–28
- Kimura H, Braun R D, Ong E T, Hsu R, Secomb T W, Papahadjopoulos D, Hong K and Dewhirst M W 1996 Fluctuations in red cell flux in tumor microvessels can lead to transient hypoxia and reoxygenation in tumor parenchyma *Cancer Res.* **56** 5522–8
- Krishna M C *et al* 2002 Overhauser enhanced magnetic resonance imaging for tumor oximetry: coregistration of tumor anatomy and tissue oxygen concentration *Proc. Natl Acad. Sci. USA* **99** 2216–21
- Krüger G and Glover G H 2001 Physiological noise in oxygenation-sensitive magnetic resonance imaging *Magn. Reson. Med.* **46** 631–7
- Lebon V, Carlier P G, Brillault-Salvat C and Leroy-Willig A 1998 Simultaneous measurement of perfusion and oxygenation changes using a multiple gradient-echo sequence: application to human muscle study *Magn. Reson. Imaging* **16** 721–9
- Milas L, Hunter N, Mason K and Withers H R 1974 Immunological resistance to pulmonary metastases in C3Hf/Bu mice bearing syngeneic fibrosarcoma of different sizes *Cancer Res.* **34** 61–67
- Mollica F, Jain R K and Netti P A 2003 A model for temporal heterogeneities of tumor blood flow *Microvasc. Res.* **65** 56–60
- Neeman M, Dafni H, Bukhari O, Braun R D and Dewhirst M W 2001 *In vivo* BOLD contrast MRI mapping of subcutaneous vascular function and maturation: validation by intravital microscopy *Magn. Reson. Med.* **45** 887–98
- Ogawa S, Lee T M, Kay A R and Tank D W 1990 Brain magnetic resonance imaging with contrast dependent on blood oxygenation *Proc. Natl Acad. Sci. USA* **87** 9868–72
- Patan S, Munn L L and Jain R K 1996 Intussusceptive microvascular growth in a human colon adenocarcinoma xenograft: a novel mechanism of tumor angiogenesis *Microvasc. Res.* **51** 260–72
- Port M, Corot C, Raynal I, Idee J M, Dencausse A, Lancelot E, Meyer D, Bonnemain B and Lautrou J 2001 Physicochemical and biological evaluation of P792, a rapid-clearance blood-pool agent for magnetic resonance imaging *Invest. Radiol.* **36** 445–54
- Pradel C *et al* 2003 Reduced capillary perfusion and permeability in human tumour xenografts treated with the VEGF signalling inhibitor ZD4190: an *in vivo* assessment using dynamic MR imaging and macromolecular contrast media *Magn. Reson. Imaging* **21** 845–51
- Proakis J G and Manolakis D G 1988 *Introduction to Digital Signal Processing* (New York: Macmillan) pp 795–841
- Robinson S P, Rodrigues L M, Ojugo A S, McSheehy P M, Howe F A and Griffiths J R 1997 The response to carbogen breathing in experimental tumour models monitored by gradient-recalled echo magnetic resonance imaging *Br. J. Cancer* **75** 1000–6
- Rofstad E K and Maseide K 1999 Radiobiological and immunohistochemical assessment of hypoxia in human melanoma xenografts: acute and chronic hypoxia in individual tumours *Int. J. Radiat. Biol.* **75** 1377–93
- Secomb T W, Hsu R, Braun R D, Ross J R, Gross J F and Dewhirst M W 1998 Theoretical simulation of oxygen transport to tumors by three-dimensional networks of microvessels *Adv. Exp. Med. Biol.* **454** 629–34

- Smith A M, Lewis B K, Ruttimann U E, Ye F Q, Sinnwell T M, Yang Y, Duyn J H and Frank J A 1999 Investigation of low frequency drift in fMRI signal *Neuroimage* **9** 526–33
- Taylor J S and Reddick W E 2000 Evolution from empirical dynamic contrast-enhanced magnetic resonance imaging to pharmacokinetic MRI *Adv. Drug. Deliv. Rev.* **41** 91–110
- Thomlinson R H and Gray L H 1955 The histological structure of some human lung cancers and the possible implications for radiotherapy *Br. J. Cancer* **9** 539–49
- Tofts P S 1997 Modeling tracer kinetics in dynamic Gd-DTPA MR imaging *J. Magn. Reson. Imaging* **7** 91–101
- Tofts P S *et al* 1999 Estimating kinetic parameters from dynamic contrast-enhanced T(1)-weighted MRI of a diffusable tracer: standardized quantities and symbols *J. Magn. Reson. Imaging* **10** 223–32
- Trotter M J, Chaplin D J, Durand R E and Olive P L 1989 The use of fluorescent probes to identify regions of transient perfusion in murine tumors *Int. J. Radiat. Oncol. Biol. Phys.* **16** 931–4
- Turetschek K, Floyd E, Shames D M, Roberts T P, Preda A, Novikov V, Corot C, Carter W O and Brasch R C 2001 Assessment of a rapid clearance blood pool MR contrast medium (P792) for assays of microvascular characteristics in experimental breast tumors with correlations to histopathology *Magn. Reson. Med.* **45** 880–6
- Van Cruchten S and Van Den Broeck W 2002 Morphological and biochemical aspects of apoptosis, oncosis and necrosis *Anat Histol Embryol.* **31** 214–23
- Windischberger C, Langenberger H, Sycha T, Tschernko E M, Fuchsjäger-Mayerl G, Schmetterer L and Moser E 2002 On the origin of respiratory artifacts in BOLD-EPI of the human brain *Magn. Reson. Imaging* **20** 575–82
- Wood P J and Hirst D G 1988 Cinnarizine flunarizine as radiation sensitisers in two murine tumours *Br. J. Cancer* **58** 742–5